Electromagnetic analysis of the Interspace Afocal Module of the Wide Angle Viewing System diagnostic for ITER

A. Fernández [a,c,*], J. Martínez-Fernández [a], M. Medrano [a], S. Cabrera [a], F. Le Guern [b], E. Rodríguez [c]

[a] *Laboratorio Nacional de Fusión, CIEMAT, 28040 Madrid, Spain*
[b] *F4E, Josep Pla 2, Torres Diagonal Litoral B3, 08019 Barcelona, Spain*
[c] *Department of Construction and Manufacturing Engineering, University of Oviedo, Campus de Gijón, 33203 Gijón, Spain*

ARTICLE INFO

ABSTRACT

The ITER Visible and Infrared Wide Angle Viewing System (WAVS) is a diagnostic aiming to optically monitor the tokamak first wall and divertor for machine protection, plasma control and physics analysis. The Interspace Afocal Module (IAM) is a refractive optical system, being one of the WAVS components located in the Interspace area.

In order to assure the optical performance, the IAM has to withstand all the relevant loads defined for the Final Design, including the electromagnetic (EM) loads developed in the Interspace area under EM events. Volumetric forces during transient EM events arise from the interaction of the background magnetic field with the eddy currents induced in the conductive components when they experience time-varying magnetic fields. In case of Category III and IV loads, including load combinations with certain Major Disruption and Vertical Displacement Event cases, the IAM integrity has to be ensured since its structure is classified as Safety Relevant.

The EM volumetric loads are calculated through a 3D Finite element model and will serve as inputs for the later structural analysis. The paper summarizes the EM analysis of the IAM, performed by CIEMAT, to validate its Final Design.

1. Introduction

The ITER Visible and Infrared Wide Angle Viewing System (WAVS) is a diagnostic aiming to optically monitor the tokamak first wall and divertor for machine protection, plasma control and physics analysis. The system will measure the surface temperature of plasma facing components by infrared thermography and will image the edge plasma emission in the visible range. The WAVS (ITER PBS.55.G1.C0) will be located in four Equatorial Ports (EP3, EP9, EP12 and EP17), comprising 15 lines of sight (LoS), four in each of the ports EP3, 9 and 17, and three in EP12, to survey at least 80% of the overall area of the vacuum vessel (Fig. 1) [1].

The conceptual design was presented in January 2013 and was further developed during the preliminary design phase, with a particular focus on the EP12 [2]. The EP12 has been selected as the first plasma port, being the diagnostic in this port the only one needing to be available for the ITER first plasma, planned in December 2025 [3]. The Final Design in EP12, including three lines of sight, is currently being

developed through a Specific Grant from F4E awarded to the Consortium constituted by CEA, CIEMAT, INTA and Bertin Technologies.

The Interspace Afocal Module (IAM) is one of the WAVS components located in the Interspace (IS) area (Fig. 2). The IAM consists in a refractive optical system with two doublets of lenses per LoS, which relays the pupil ahead, controlling at the same time the beam diameter [4]. The afocal sets are placed in the IAM support structure, which is directly attached to the Interspace Support Structure (ISS) (Fig. 3) [5].

In order to assure the optical performance, the IAM has to withstand all the relevant loads defined for the Final Design Review (FDR), including the electromagnetic (EM) loads developed in the IS area under EM events. Transient EM events cause the induction of eddy currents inside the conductive components, since they experience time-varying magnetic fields. Volumetric forces arise from the interaction of these induced currents with the background magnetic field, according to the Lorentz's law. In case of Category III and IV loads, including load combinations with certain Major Disruption (MD) and Vertical Displacement Event (VDE) cases, the IAM integrity has to be ensured
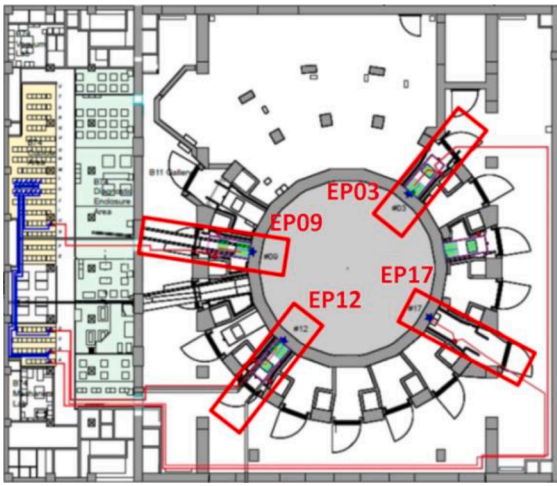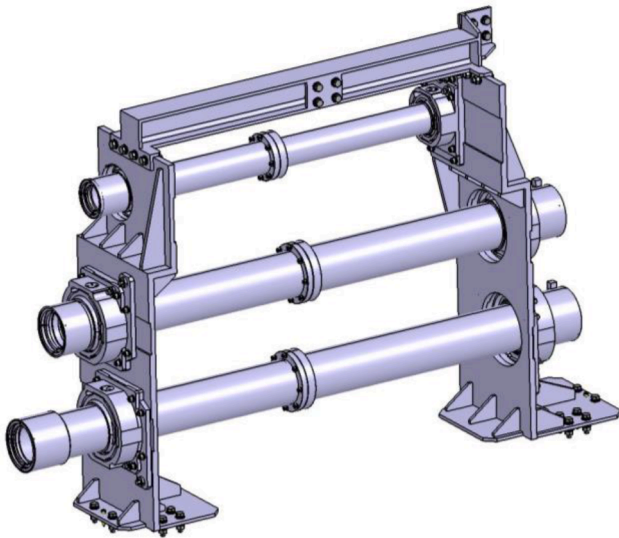

Fig. 1. WAVS general layout.

Fig. 2. Interspace Afocal Module.

since its structure is classified as Safety Relevant [6].

The EM volumetric loads have been calculated with the tool ANSYS Maxwell through a 3D Finite Element (FE) model created in the ANSYS Electronics Desktop 2021 R2. The ISS chassis and main frame structure were also included in the EM model to take into account the impact of flowing induced currents between the IAM and the ISS, to which it is attached and electrically connected. The resulting 3D map of force density vector values will be imported in the ANSYS Mechanical model, serving as an input for the later structural analysis. The paper summarizes the EM analysis performed, aiming to contribute to the validation of the IAM Final Design.

2. Electromagnetic events

2.1. Description of the fast transient EM events

The relevant EM loads in the IS are due to the following three types of fast transient EM events [7,8]:

- Major Disruptions (MDs)

They consist in a plasma thermal quench followed by a current

quench, caused by a sudden loss of the magnetic confinement and impurity influx. The thermal quench implies a fast loss of the plasma thermal energy. The current quench, a fast drop in plasma current, is often accompanied by a vertical drift and compression of the plasma core.

- Vertical Displacement Events (VDEs)

They consist in an irreversible plasma vertical drift caused by a failure of vertical position control. The plasma column starts a slow vertical drift upward or downward and then makes contact with the first wall (FW) resulting in the so-called halo currents in the FW structure. A thermal quench starts as soon as the plasma comes in contact with the FW. The plasma shape remains limited by the FW and shrinks in cross-section. Finally, a current quench is initiated.

- Magnet Fast Discharges (MFDs)

They are events where the current flowing in one or more of the ITER magnets (TF, PF, CS, CC or all) is rapidly brought to zero by means of discharge resistors, which dissipate the large stored magnetic energy. They are usually triggered by the magnet quench detection systems upon detection of a quench, in order to protect the conductors from overheating.

2.2. EM load combinations for the FDR

The loads are classified into categories (I, II, III and IV) depending on their expectation of occurrence.

The following Table 1 summarizes the considered load combinations for the structural analysis at FDR level. Note that SL-1, SL-2 and SMHV are different cases of seismic events [6,9].

The load combinations in Table 1 can be simplified as the EM effects in the IS region of MD II and MD III are the same. This is due to the fact that the current quench decay is equal between these categories. The only difference is the duration of the thermal quench [7,10,11]. Moreover, the overall worst MD event can be conservatively selected to cover all the MD cases. The same reasoning applies for VDEs.

2.3. Input data for the EM analysis

Magnetic flux density (B [T]) values in the IS region of EP12 have been calculated by ITER Organization (IO) for the different transient MD and VDE events [12]. The output data of the two worst MD events, and the two worst VDE events in the area of interest, that is, the region around the WAVS components, has been requested as inputs for the present study.

The requested four events are: MD_UP_exp16ms_catIII, MD_DW_exp16ms_catIII, VDE_UP_lin36ms and VDE_DW_slow [9].

3. Methodology and type of EM analysis

Given the maps of the magnetic field evolution in IS of the considered EM events, the EM loads can be calculated by using ad hoc EM models comprising the WAVS component studied, the IAM in this case, plus the ISS. The ISS chassis and main frame structure are included in the EM model of the IAM to take into account the impact of flowing induced currents between the component and the ISS, to which it is attached and electrically connected.

For each EM event, the worst instant during the transient, in the region of the WAVS components, was selected. The worst instant is quantitatively assessed to be the one producing the highest volumetric forces. The EM forces are proportional to the cross product of $\mathbf{j} \times \mathbf{B}$ (Lorentz Force), being $\mathbf{j}$ the current density vector, and $\mathbf{j}$ is proportional to d$\mathbf{B}$/dt, according to the Faraday-Lenz law of induction. Then, we can evaluate this instant by comparing the vector magnitude of the cross

product of (d**B**/dt) x **B**.

The model approach considers the IAM and the ISS immersed in a time-varying magnetic field defined by the constant values of **B** [T] and d**B**/dt [T/s] of the selected worst instant. The transient is simulated during a period of time long enough (typically 10-40 ms, depending on the case) for the eddy currents to develop and reach their asymptotic maximum value (see Section 6.1). This conservative approach of selecting the **B** and d**B**/dt values of the worst instant ensures that the calculated forces due to the eddy currents are the maximum possible in the full transient of the EM event. The simplifications made, considering a uniform B field in the region of interest and the worst instant in the transient, are justified because the expected resulting EM loads are not design driving (see Section 7). On the other hand, this simplified approach has the major advantage of important time savings both in the FE model preparation and in calculation time. The approach was agreed and accepted by ITER Organization and F4E [9].

The type of EM analysis to be conducted for the FDR phase corresponds to a 3D transient EM FEA calculation.

The method to perform the analysis consists in imposing time-varying current values to three spherical shells, which surround the studied components [13]. Each one creates one Cartesian component (Bx, By and Bz) of the B field (Fig. 4). These currents create a region in the central part of the spheres in which the magnetic field is uniform in the space domain but variable in time.

The thickness of the spherical shells varies with a cosinusoidal law, while the imposed current density is uniform. The total current to be applied to the section of the shell can be calculated as:

$$I_i(t) = \frac{3B_i(t)S_i}{2\mu_0 s_{i,0}} \tag{1}$$

where $B_i(t)$ is the required time-varying magnetic field in the i direction, S_i the cross section surface of the shell as highlighted in Fig. 5, $\mu_0 = 4\pi * 10^{-7} \, N/A^2$ the vacuum permeability and $s_{i,0}$ the shell equatorial thickness [13]. The method has been verified in [13].

A superimposed cubic vacuum region is created around the spheres with 200% padding in all directions.

Finally, for the later structural analysis, the calculated volumetric forces will be fully imported in the ANSYS Mechanical FE model. This procedure ensures the accuracy of the mechanical results.

4. Description of FE analysis

4.1. Identification of the worst case scenarios

For the identification of the worst case scenarios, the events have been compared through the value of $||(dB/dt) \times B||$ in the worst instant of each transient. In order to do that, a representative point in the region of the WAVS components has been defined for the evaluation of the transient B field.

The coordinate system used is defined for EP12 (EP12CS). The origin is in the center of the ITER tokamak, being the same origin as in the Tokamak Global Coordinate System (TGCS). The X axis is in the radial direction of EP12, rotated 230º with respect to the X axis in TGCS [14]. The Y axis is in the toroidal direction and the Z axis is in the vertical direction.
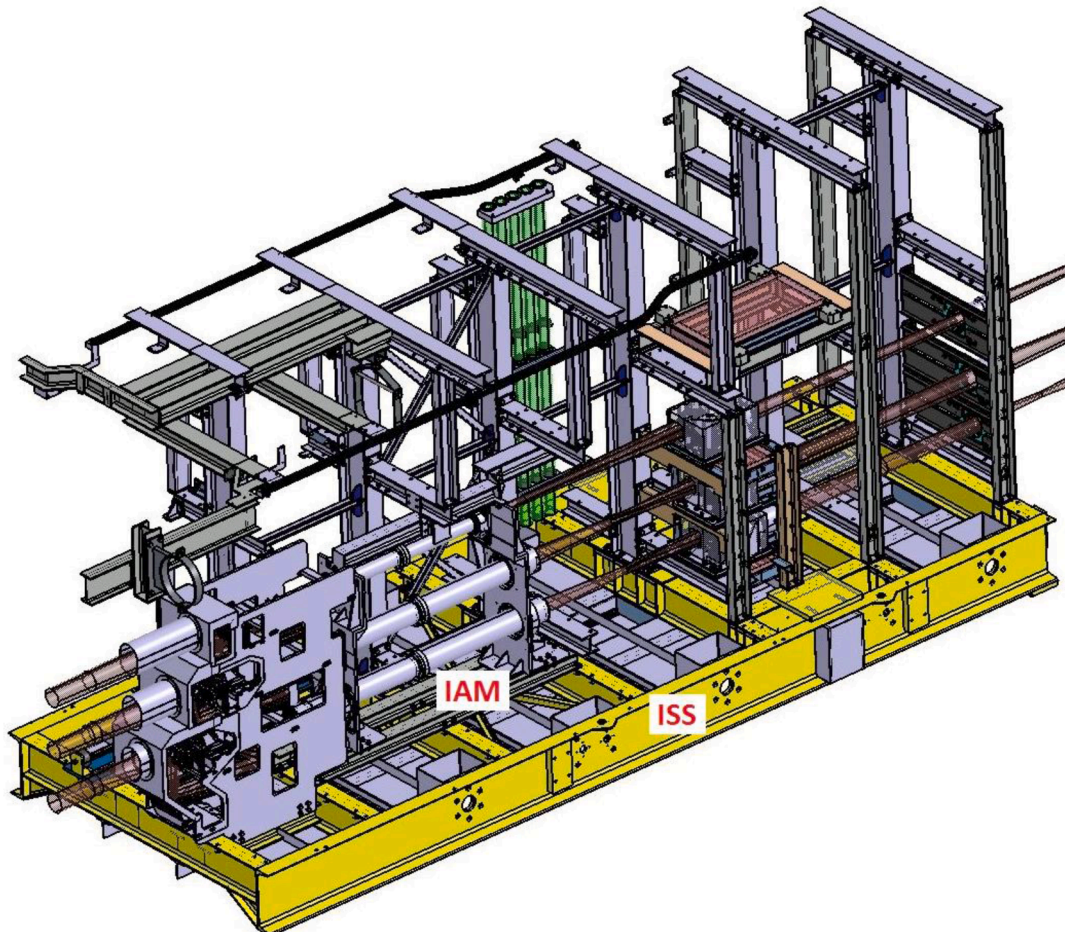

Fig. 3. Integration view of the WAVS components with the ISS in EP12.

Table 1
Applicable load combination to 55.G1.C0 Ex-Vessel components for FDR.

Pressure	Seismic	Plasma	Others CatI[1]	Others CatII[1]	Others CatIII[1]	Others CatIV[1]	Cat	# of events[2]
Testing, Assembly[1]							-	-
Normal Operation[1]							I	30000
Baking conditions[1]							I	500
		MD I	P				I	2600[3]
		MD II	P	P			II	400[3]
		VDE II	P	P			II	300[3]
	SL-1		P	P			II	1[4][5]
	SL-1	MD I	P	P			II	1[4][5]
		MD III	P	P	P		III	-
		VDE III	P	P	P		III	-
	SL-1	MD II	P	P	P		III	-(5)
	SL-1	VDE II	P	P	P		III	-(5)
	SMHV		P	P	P		III	-(5)
LOCA_PC III			P	P	P		III	-(6)
		VDE IV	P	P	P	P	IV[7]	-
		MD IV	P	P	P	P	IV[7]	-
	SL-1	MD III	P	P	P	P	IV[7]	-(5)
Int. fire			P	P	P	P	IV[7]	-(5)
	SL-2		P	P	P	P	IV	-(5)

[1] Other load conditions, which are peculiar (P) to a particular port. It includes dead weight, thermal loads, interface loads, etc.

[2] Unless a detailed dynamic analysis is performed and the number of cycles per event is directly calculated, it is recommended to assume for each seismic event 10 equivalent maximum stress cycles whenever a fatigue or a cyclic load analysis is required. Conservatively, for disruptions and VDEs the number of equivalent cycles per event should be assumed to be 5, as a way to cope with the uncertainty linked to VDE events. Category III events and combinations shall be assumed to occur once in the machine life unless otherwise specified.

[3] This number is reduced if this event is combined with other events (examples MD + MFD, MD + ICE, etc.). The reduction corresponds to the number of events assumed in the additional combinations.

[4] As this event has a return period of more than 100 years it is expected to occur only once in the machine life. If required by investment protections it shall be assumed to occur a maximum number of 5 times (to be clarify after the PDR).

[5] Seismic events may occur during baking.

[6] During an accident as Loss-of-Coolant Accident (LOCA), these thermal and pressure loads shall be applied in the direction to increase the stresses. Please, note that LOCA could occur during baking.

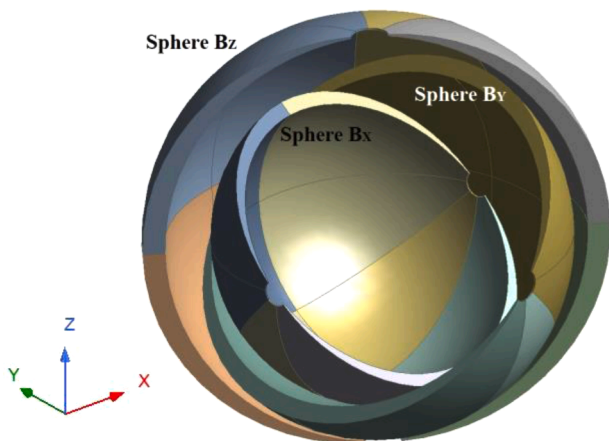[7] Only for safety relevant components.

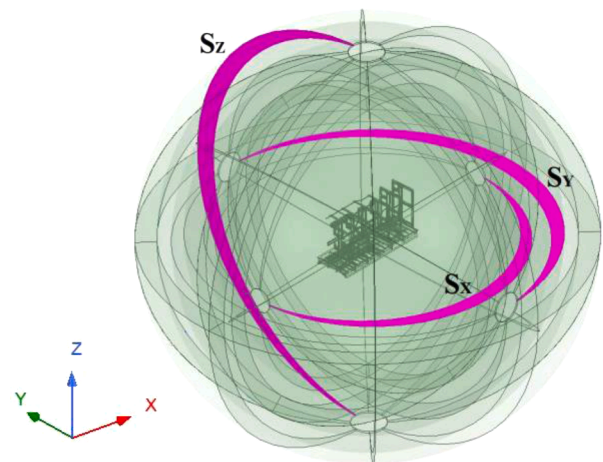**Fig. 4.** Geometry model of the spherical shells (sections view).

Fig. 5. Spheres cross sections where the currents are imposed.

Initially, the center of gravity of the system composed by the main WAVS components (OH-ORU plus IAM) was selected as the representative point for the B field evaluation. This point corresponds to X = 13.174 m, Y = -0.378 m and Z = 0.205 m. In order to check that the B field does not vary significantly across the region of interest, the spatial variation of the B field has been plotted for each event at the initial time. The four events behave in a similar way, so the extracted qualitative conclusions are the same for all of them. The vector magnitude of the B field varies significantly in the radial (X) direction, increasing in magnitude towards the tokamak origin (Fig. 6). As the main WAVS components are placed in the first meters of the IS, up to X = 15 m, and

the transient variation of B is similar in the region of interest, the lowest value of X in the ISS, X = 12.185 m, has been conservatively selected for the B field evaluation of all the events. On the other hand, the variation in the toroidal (Y) and vertical (Z) directions is negligible or small in the region of the WAVS components, that is, for -0.610 m < Y < -0.173 m and -0.560 m < Z < 0.966 m (Fig. 7 and Fig. 8). Therefore, the Y and Z coordinates of the center of gravity of the mentioned system have been considered acceptable.

The four events have been evaluated in the selected point: X = 12.185 m, Y = -0.378 m and Z = 0.205 m (Fig. 9). From the transients
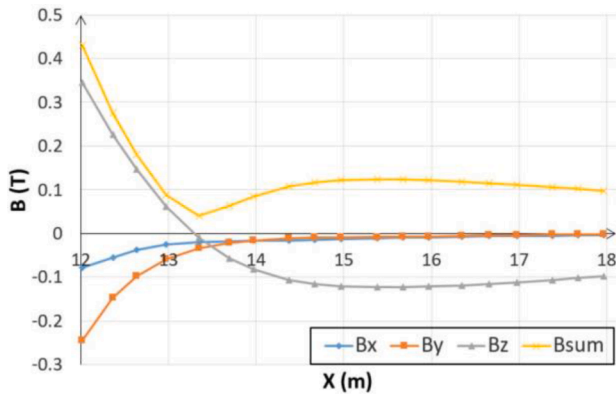
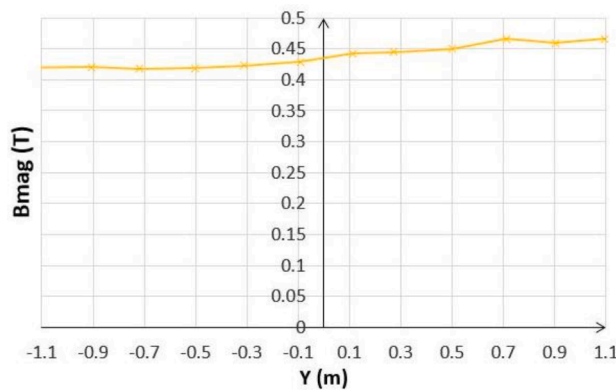**Fig. 6.** Radial variation of **B** in the IS region for MD_DW_exp16ms_catIII at t = 0 s.

Fig. 9. Point selected (red circle) for evaluation of the transient EM events.

Fig. 7. B variation along Y in the IS region for MD_DW_exp16ms_catIII at t = 0 s.
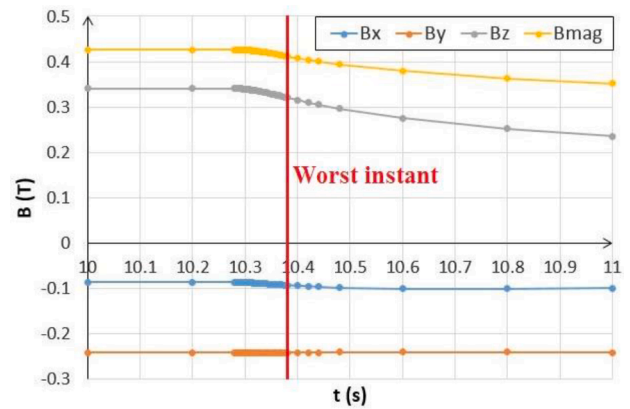
Fig. 10. B evolution of MD_DW_exp16ms_catIII in the selected representative point.

Table 2
$||\mathbf{B}||$, $||d\mathbf{B}/dt||$ and $||(d\mathbf{B}/dt)\mathrm{x}\mathbf{B}||$ in the worst instant of each EM event.

EM event	$||\mathbf{B}||$ [T]	$||d\mathbf{B}/dt||$ [T/s]	$||(d\mathbf{B}/dt)\mathrm{x}\mathbf{B}||$ [T²/s]
MD_UP_exp16ms_catIII	0.347	0.239	0.061
MD_DW_exp16ms_catIII	0.412	0.312	0.091
VDE_UP_lin36ms	0.342	0.162	0.046
VDE_DW_slow	0.330	0.187	0.046

Fig. 8. Vertical variation of B in the IS region for MD_DW_exp16ms_catIII at t = 0 s.

Table 3
B and dB/dt component values for the worst instant of MD_DW_exp16ms_catIII.

Parameter	Vector component		
	X	Y	Z
B [T]	-0.093	-0.242	0.320
dB/dt [T/s]	-0.075	0.002	-0.303

obtained (Fig. 10), the $||(d\mathbf{B}/dt) \mathrm{x} \mathbf{B}||$ values for the worst instant have been extracted and compared (Table 2). The Category III Major Disruption MD_DW_exp16ms_catIII is the worst event in the area of interest, having the highest $||(d\mathbf{B}/dt) \mathrm{x} \mathbf{B}||$ value in the worst instant. Being the worst event a MD case, it envelops all the cases in the applicable load combinations, including the category IV loads. On the other hand, not all the MD cases are enveloped by VDEs, as can be seen in Table 1.

The **B** and d**B**/dt values by components in the worst instant of MD_DW_exp16ms_catIII will be used as inputs for the EM analysis (Table 3).
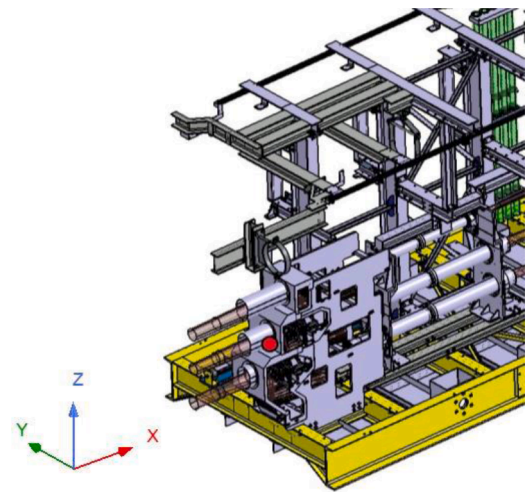
4.2. Material properties

The electrical properties for the structural materials of the components were taken from the "ITER Material Properties Handbook" [15, 16]. Room temperature of 20ºC is considered for the properties evaluation (Table 4). The structural material of the WAVS components is Stainless Steel 316L(N)-IG. The material of both, the ISS chassis and main frame, is Stainless Steel 316L [17].

Table 4

Materials electrical properties at 20ºC.

Material	Electrical resistivity [Ωm]	Relative permeability
SS316L(N)-IG	$7.50 \bullet 10^{-7}$	1
SS316L	$7.76 \bullet 10^{-7}$	1

4.3. Geometry model in ANSYS

The ENOVIA geometry model draft versions of the IAM, ISS chassis and ISS main frame structure were imported in ANSYS. The ANSYS tools DesignModeler and SpaceClaim were used for geometry simplification and healing of the imported models. As stated before, the ISS chassis and main frame structure have been included in the EM FE model (Maxwell model) to take into account the impact of flowing induced currents between the IAM and the ISS (Fig. 11).

The geometry model of IAM has been divided in subcomponents to ease the analysis of the EM loads by parts. Further subdivisions have been performed in an iterative process after checking the preliminary results of the analysis. These subdivisions allow to apply local mesh refinements in regions with high variation of eddy currents. Specifically, the upper beam has been cut around the middle interface, another cut was performed around the interface of the rear leg, and the shafts of all the gimbals were separated from the rest (Fig. 12).

The geometry of the components was simplified in the FE models, removing those elements and geometrical details that are not relevant for the EM analysis. All pins, bolts and screws were removed, and the corresponding holes were filled. The structural bolts and screws will be included in the model for the later structural analysis. Only the electrical conductive elements were modelled, i.e. the elements made of stainless steel 316L or 316L(N)-IG, as the rest do not interact with the magnetic field and are no relevant for this analysis. Perfect conductivity is assumed between parts with electrical contact.

The volume of the IAM as measured from CAD files has been verified to correspond to that of the FE model with a similarity above 99% (Table 5).

4.4. FE mesh

The allowed mesh elements in Maxwell 3D are tetrahedrons [18]. The maximum element size for each part has been selected according to the required local solution accuracy. An iterative process was followed for the local mesh refinements. In addition, mesh sensitivity analyses were performed to check the validity of the model mesh (Section 6).
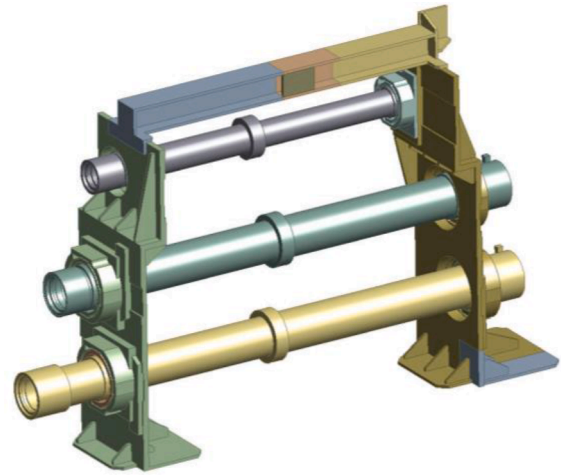

Fig. 12. Geometry model of IAM.

Table 5

Volume check of the IAM FE model.

	Volume CAD [m^3]	Volume FE model [m^3]	Difference [%]
IAM	0.05221	0.05246	0.48

Mesh quality was assured by improving the following mesh parameters with respect to the default values. The maximum surface deviation was reduced down to 1.5 mm for the IAM parts and to 80 mm for the ISS. The maximum aspect ratio of the triangles was set to 2 for the IAM parts and to 5 for the ISS, being 10 the default value [19]. The Maxwell mesh feedback analysis tool was run to check that there were no errors in the created mesh (Fig. 13 and Fig. 14).

The final mesh statistics of the baseline model are reported in the following Table 6.

In addition, the global accuracy of the solution for the created mesh was measured by means of the energy error parameter in Maxwell [18]. The default target value for the energy error in Maxwell 3D is 1%, while a conservative target value could be set in 0.01%, as chosen in a similar EM analysis of an ITER diagnostic [20]. The energy error obtained for the baseline simulation was 0.0015%, much lower than the conservative target of 0.01%. This result confirms the suitability of the created mesh.
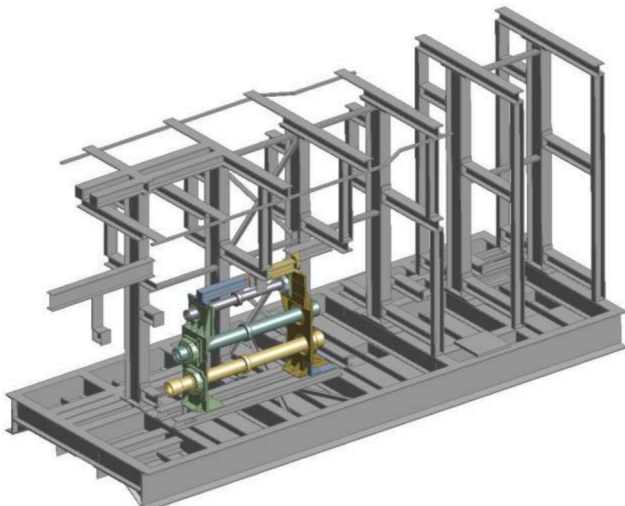

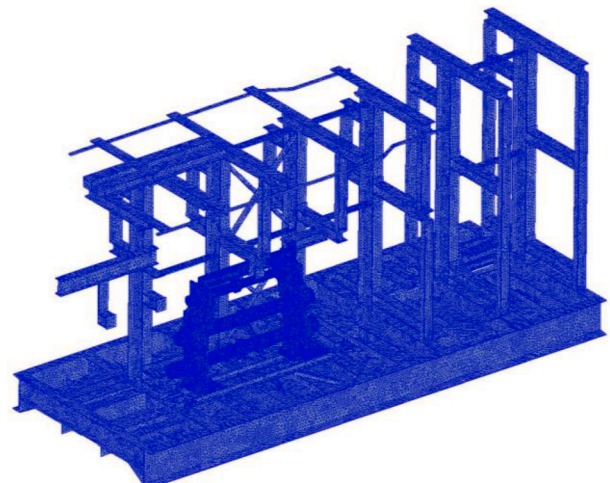
Fig. 11. Geometry model of IAM with the ISS.

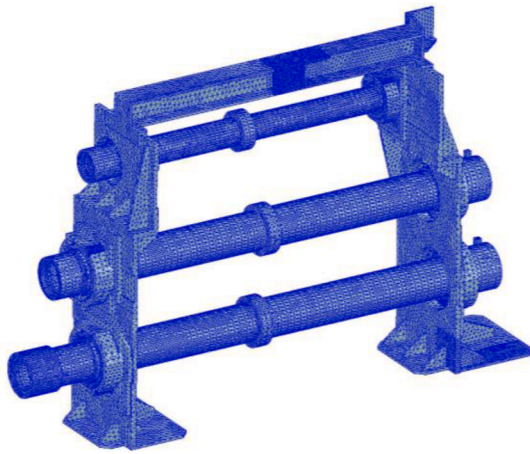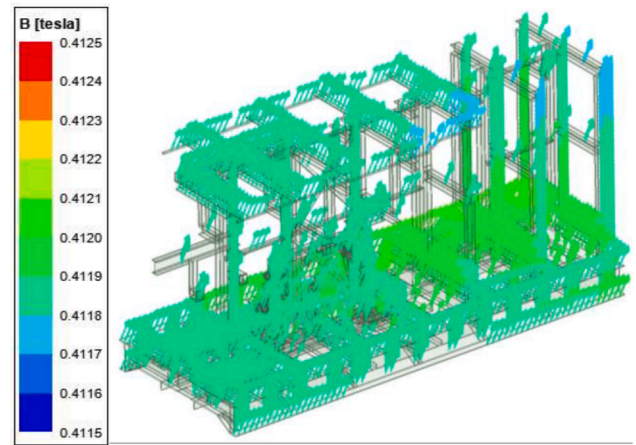**Fig. 13.** Model mesh of IAM with the ISS.

Fig. 14. Model mesh of IAM.

Table 6
Mesh statistics of the baseline model.

Model component	Max. element size [mm]	Number of mesh elements
IAM	4 to 25	398 286
ISS	50	431 112
Spheres	800 to 1 120	192 831
Region	6 000	1 428 347
Total	-	2 450 576

4.5. Calculation of the required B field

As the variation of the B field in the present EM analysis is linear, the equation for the input current to be imposed to the spherical shells (1) can be written as:

$$I_i(t) = \frac{3S_i}{2\mu_0 s_{i,0}} \left(B_{i,0} + \frac{dB_i}{dt} t \right) \quad (2)$$

Introducing in (2) the $B_{i,0}$ and dB_i/dt values from Table 3, together with the corresponding S_i and $s_{i,0}$ parameters of each spherical shell, we obtain the following equations as input for the imposed current in the spheres:

$$I_X(t) = 21\ 346\ 046(-0.093 - 0.075t) \quad (3)$$

$$I_Y(t) = 25\ 712\ 365(-0.242 + 0.002t) \quad (4)$$

$$I_Z(t) = 29\ 997\ 865(0.320 - 0.303t) \quad (5)$$

However, these input curves introduce a small error in the calculated B field due to a number of causes as the FE discretization of the spheres and the holes introduced in the upper and lower parts of the spheres (Fig. 4 and Fig. 5). These holes are necessary to ease the mesh generation and for numerical stability of the solution. After checking the obtained error for the initial B field in each direction i, a correction factor has been introduced for each of the Eqs. (3), (4) and (5). The correction factors introduced are: $f_X = 1.00308$, $f_Y = 1.00171$, $f_Z = 0.99913$.

The obtained B field distribution was compared to the required initial B field in the IS region. The target uniform magnitude of 0.412 T (Table 2) was reached with a maximum deviation of ±0.3 mT, corresponding to a relative error of 0.07% (Fig. 15).

5. Results

5.1. Eddy currents

The resulting current loops lie mainly in the horizontal plane (anti-clockwise) of the ISS, because the major field variation is due to the

Fig. 15. B field in the IS at t=0 s.

vertical component (negative variation), as the Faraday-Lenz law predicts (Fig. 16 and Fig. 17).

The calculated current density peak in the IAM, 527.8 kA/m², is given in the mid-upper interface of the IAM with the ISS, where a high current goes through a narrow section (Fig. 18).

5.2. Volumetric forces

The calculated main forces in the IAM are in the plane YZ, in the diagonal direction of -Y, -Z (Fig. 19), as a result of the product **j** x **B** (Lorentz force). This is due to the fact that the main currents go in the positive direction of X and the direction of the B field is mainly in the YZ plane, in the diagonal of –Y, +Z.

The calculated force density peak in the IAM is 183.4 kN/m³ (Fig. 20). The peak is given in the same position of the current density peak.

The calculated total force in the IAM is 205.8 N. The calculated total torque in the IAM, with respect to its center of gravity, is 35.7 Nm (Table 7).

6. Verification of the FE analysis

6.1. Sensitivity analyses

The accuracy of the results was verified by performing the following sensitivity analyses: mesh sensitivity of the spheres, ISS and IAM; time step sensitivity and total time sensitivity.

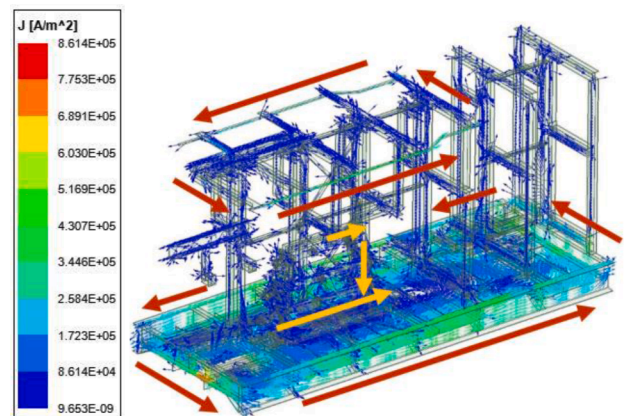The ITER requirement is to keep the results within a 5% relative error

Fig. 16. Eddy currents in IAM and ISS at t=30 ms. Main current paths in yellow for the IAM and red for the ISS.
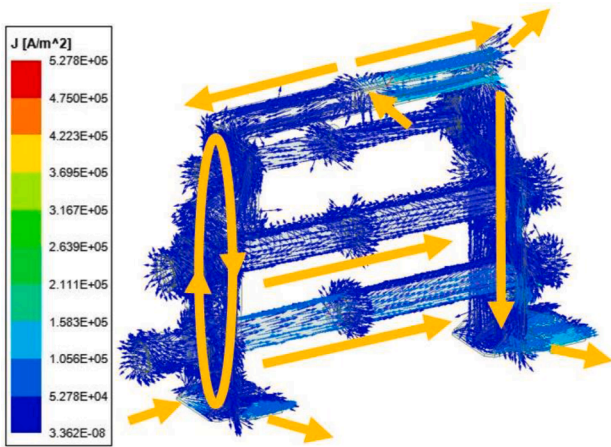
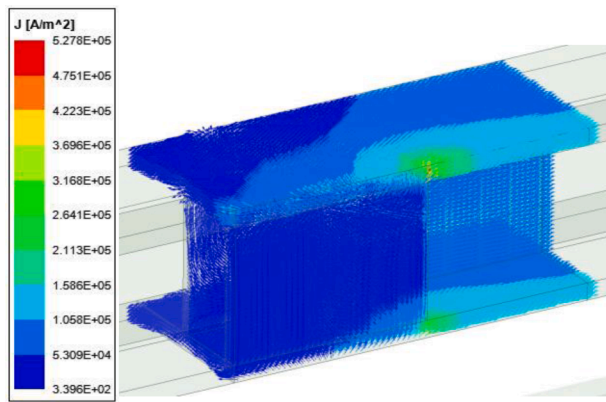**Fig. 17.** Eddy currents in IAM at t=30 ms. Main current paths in yellow.

Fig. 18. Eddy currents in the mid-upper interface of the IAM with the ISS at t=30 ms.
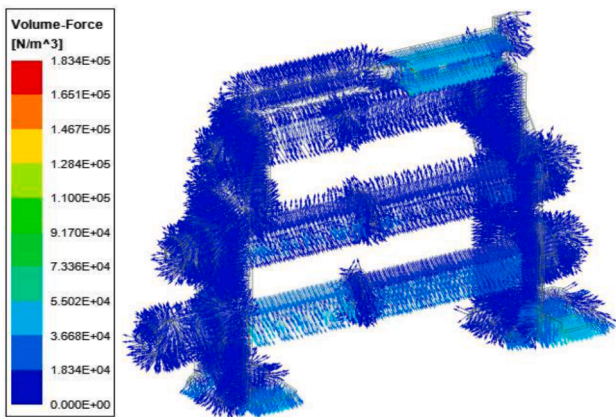

Fig. 19. Volumetric forces in the IAM at t=30 ms.

for each of the analyses [21]. The error for a given case is calculated with respect to the case with the most accurate result. The resulting relative errors were kept under 2.6% for the total force and torque in IAM in all the analyses.

In the performed mesh sensitivity analyses of IAM and ISS, the number of mesh elements was doubled for each of the components in independent simulations (Table 8). In the mesh sensitivity analysis of the spheres, the maximum element size in them was divided by two, increasing the number of elements in the spheres by a factor close to 5.
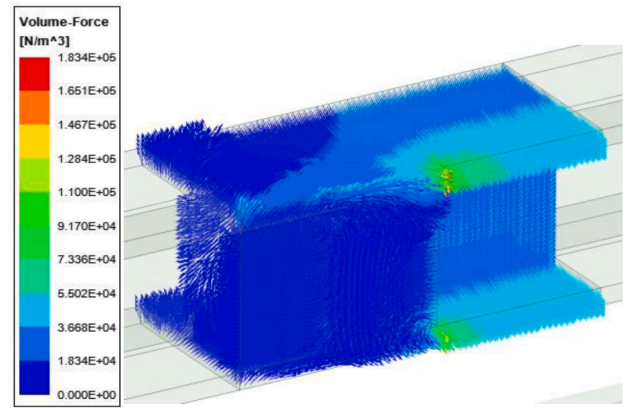

Fig. 20. Volumetric forces in the in the mid-upper interface of the IAM with the ISS at t=30 ms.

Table 7
Calculated total force (in TGCS) and torque (in EP12CS) in the IAM.

Parameter	Vector component			Vector magnitude
	X	Y	Z	
F (N)	-71.0	-141.1	-131.8	205.8
T (Nm)	-12.3	23.8	-23.6	35.7

Table 8
Mesh sensitivity analyses results.

Mesh modified for component	Max. element size [mm]	Number of mesh elements	F [N]	T [Nm]
IAM	1 to 25	937 357	207.0	35.5
ISS	35	832 243	205.8	35.6

The maximum deviation of B in IS was reduced down to ±0.1 mT.

In the time step sensitivity analysis the initial time step of 1 ms was doubled. As the error obtained was well under the requirement, a 2 ms step was selected for the baseline simulation. In the total time sensitivity analysis the results of a simulation with a total period of 30 ms were compared to the results of a simulation with 40 ms. As the error was about 2%, a total time of 30 ms was selected as baseline (Fig. 21 and Fig. 22).
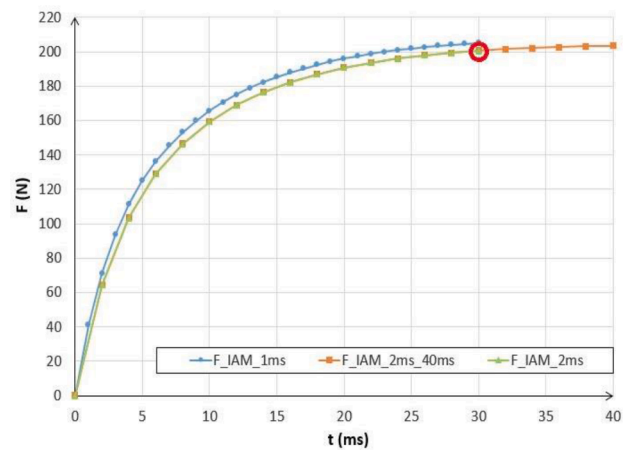

Fig. 21. Time step and total time sensitivity analyses for the total force in the IAM. Selected total time in red circle.
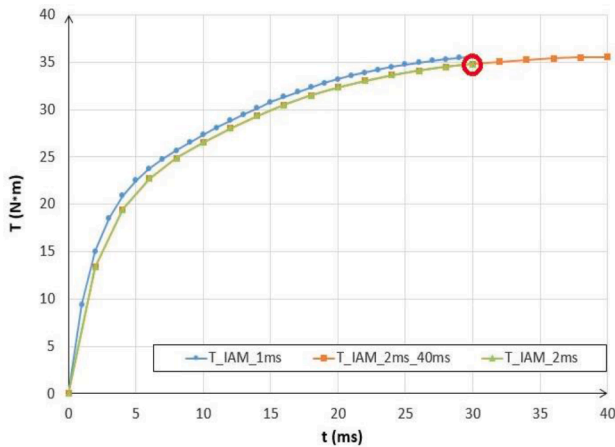
Fig. 22. Time step and total time sensitivity analyses for the total torque in the IAM. Selected total time in red circle.

6.2. Study of the current and force peak singularity

Performing a local mesh sensitivity analysis for the region of the current density and volumetric force peaks, a field singularity was identified [22]. The resulting local current density and volumetric force do not converge and continue to increase when the mesh is progressively refined (Fig. 23). This seems to be because the magnetic field does not
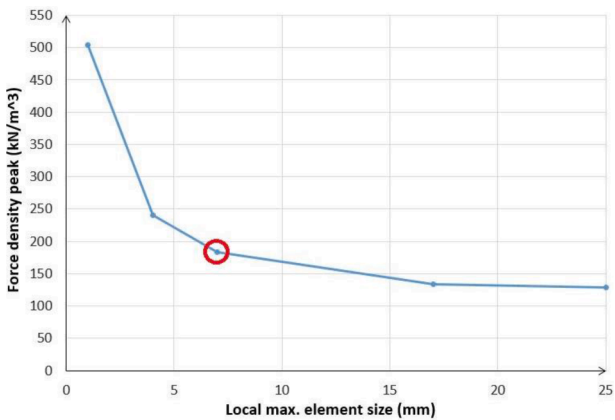

Fig. 23. Volumetric forces in the mid-upper interface of the IAM with the ISS at t=30 m.
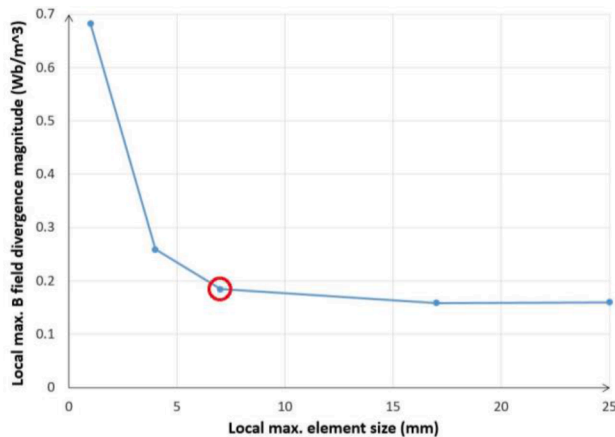

Fig. 24. Local divergence of B Vs. local element size for the region of the force peak. Maximum local element size selected in red circle.

converge in sharp inner boundary corners. This issue is documented in [23] for a T-Omega formulation of the FE method, as it is the case in Maxwell 3D transient simulations.

One hint of the presumed convergence errors in sharp inner boundary corners or edges lies in the value of the divergence of B in these boundaries. This seems to be related to the impossibility to fulfill both the boundary conditions and the equation from the T-Omega formulation at the same time [23]. As the latter is only enforced in a weak way as per the Galerkin method employed in the FE analysis, the divergence of B separates itself from 0. As happens with the peak force, the divergence of B continues to increase when the mesh is progressively refined. Therefore, the local error in the solution seems to increase when refining the mesh. Thus, the most conservative solution was chosen before the explosion of the error, that is, the simulation with the minimum local element size still providing acceptable results (Fig. 24).

7. Conclusions

The EM analysis of the IAM at FDR level has been performed. A 3D ANSYS Maxwell FEM model has been developed, including the ISS to take into account the flowing eddy currents between the IAM and the structure.

Sensitivity analyses have been carried out to ensure the accuracy of the results.

The method implemented, by using spherical shells to create a region where the B field is uniform, is considered appropriate if the resulting EM loads are not design driving loads. In that case, the error derived from the simplification is acceptable. This condition is met if the loads are in the same order of magnitude or less than the self weight of IAM [9]. Indeed, the total EM force in the IAM is 205.8 N, a factor 20 less than the self weight, 4 081.7 N. The maximum force density locally reached is 183 400 N/m^3, being in the same order of magnitude than the weight density, 77 793 N/m^3. These values confirm the suitability of the method.

The results of the EM analysis are sound with the expected values and with the physical laws governing the studied phenomena. As the results confirm that both, the local volumetric forces and the total force in the IAM are not design driving loads, can be concluded that the EM events will not compromise this final design of the IAM.

Disclaimer

Declaration of Competing Interest

The authors declare that they have no known competing financial interests or personal relationships that could have appeared to influence the work reported in this paper.

Data availability

Data will be made available on request.

References

[1] Reichle, et al., Concept development for the ITER equatorial port visible/infrared wide angle viewing system, Rev. Sci. Instrum. 83 (2012) 10E520, https://doi.org/10.1063/1.4734487.

[2] L. Letellier, et al., System level design of the ITER equatorial visible/infrared wide angle viewing system, Fusion Eng. Des. 123 (2017), 650653, https://doi.org/10.1016/j.fusengdes.2017.06.005.

[3] B. Bigot, ITER assembly phase: progress toward first plasma, Fusion Eng. Des. 164 (2021), 112207, https://doi.org/10.1016/j.fusengdes.2020.112207.

[4] C. Pastor, et al., Optical design of ex vessel components for the Wide Angle Viewing System diagnostic for ITER, Fusion Eng. Des. 168 (2021), 112607, https://doi.org/10.1016/j.fusengdes.2021.112607.

[5] M. Medrano, et al., Design overview of ex vessel components for the Wide Angle Viewing System diagnostic for ITER Equatorial Port 12, Fusion Eng. Des. 168 (2021), 112651, https://doi.org/10.1016/j.fusengdes.2021.112651.

[6] F. Le Guern et al., 55.G1.C0_System Load Specification(s) for ex-vessel components, ITER IDM Report (3M2DEZ v1.2), 2021.

[7] P. Testoni, et al., F4E studies for the electromagnetic analysis of ITER components, Fusion Eng. Des. 89 (2014) 1854–1858, https://doi.org/10.1016/j.fusengdes.2014.01.082.

[8] G. Sannazzaro et al., Load Specifications (LS), ITER IDM report (222QGL v6.2), 2017.

[9] A. Fernández et al., Analysis plan for non PIC ex-vessel components of 55.G1.C0 at FDR level (Electromagnetic), F4E IDM Report (2RQZPU v1.0), 2022.

[10] P. Testoni et al., Manual for ITER electro-magnetic analyses, ITER IDM report (SYC9KF v1.0), 2016.

[11] M. Kocan et al., 03_Minutes & Actions_55.G1_Vis/IR_Exvessel_SLS/Analysis_FDR, ITER IDM Report (4NKL5F v1.0), 2021.

[12] S. Iglesias et al., EM analysis of ISS (Eq12), ITER IDM report (4FYSR5 v1.0), 2020.

[13] S. Garitta, et al., Electromagnetic analysis of ITER equatorial Wide Angle Viewing System (WAVS) in-vessel components, Fusion Eng. Des. 170 (2021), 112471, https://doi.org/10.1016/j.fusengdes.2021.112471.

[14] J. Pavageau et al., ITER coordinate systems, ITER IDM report (2A9PXZ v3.7), 2008.

[15] V. Barabash et al., AA04-3201 316L (N)-IG stainless steel – electrical resistivity, ITER IDM report (222W3R v3.1), 2008.

[16] V. Barabash et al., 316 L - electrical resistivity, ITER IDM report (222UTC v1.0), 2005.

[17] O. Chauveau et al., 55.QC - Bill of Materials (BOM) and system components classification, ITER IDM report (UZTYB3 v1.3), 2020.

[18] ANSYS Maxwell Help, ANSYS Inc., Release 2021 R2, 2021, https://ansyshelp.ansys.com/Views/Secured/Electronics/v212/en/PDFs/Maxwell.pdf.

[19] ANSYS Maxwell 3D v15, User's Guide, ANSYS Inc., 2012. http://ansoft-maxwell.narod.ru/en/CompleteMaxwell3D_V15.pdf.

[20] D. Giorla, et al., EM zooming procedure in ANSYS Maxwell 3D, Fusion Eng. Des. 132 (2018) 67–72, https://doi.org/10.1016/j.fusengdes.2018.04.096.

[21] R. Roccella et al., Guideline for electromagnetic analyses, ITER IDM report (33UCBG v2.1), 2015.

[22] P. Testoni et al., F4E QA-114 guideline for electromagnetic analyses, F4E IDM report (2HWW2N v1.1). 2019.

[23] K. Preis, et al., Gauged current vector potential and reentrant corners in the FEM analysis of 3D eddy currents, IEEE Trans. Magn. 36 (4) (2000). https://ieeexplore.ieee.org/document/877575.